Polarization-Multiplexed DMT With IM-DD Using 2 × 2 MIMO Processing Based on SOP Estimation and MPBI Elimination
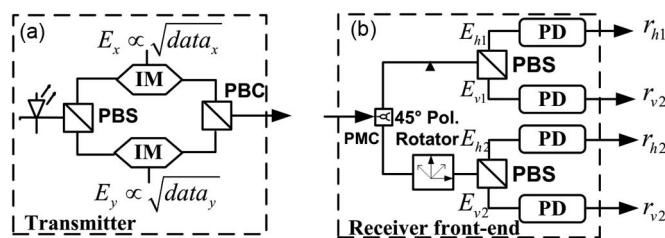
Xian Zhou, Member, IEEE
Kangping Zhong
Jiahao Huo
Jinhui Yuan
Feng Li
Liang Wang
Keping Long, Senior Member, IEEE
Alan Pak Tao Lau
Chao Lu, Member, IEEE

Polarization-Multiplexed DMT With IM-DD Using 2 × 2 MIMO Processing Based on SOP Estimation and MPBI Elimination

Xian Zhou,[1,2] *Member, IEEE*, Kangping Zhong,[1,2] Jiahao Huo,[1]
Jinhui Yuan,[2] Feng Li,[2] Liang Wang,[2] Keping Long,[1] *Senior Member, IEEE*,
Alan Pak Tao Lau,[3] and Chao Lu,[2] *Member, IEEE*

[1]School of Computer and Communication Engineering, University of Science and
Technology Beijing (USTB), Beijing 100083, China
[2]Photonics Research Centre, Department of Electronic and Information Engineering,
The Hong Kong Polytechnic University, Kowloon, Hong Kong
[3]Photonics Research Centre, Department of Electrical Engineering,
The Hong Kong Polytechnic University, Kowloon, Hong Kong

Abstract: A simple polarization-multiplexed (PM) discrete multitone (DMT) system with
intensity modulation and direct detection (IM-DD) is proposed for short-reach optical
communications. Only four photodetectors (PDs) are required at the receiver, and no ex-
tra 90° hybrid and balanced detection is necessary. Novel digital signal processing
(DSP) algorithms are proposed for state-of-polarization (SOP) estimation and subse-
quent mixed polarization beat interference (MPBI) elimination. These enable polariza-
tion demultiplexing and channel estimation to be implemented by a simple 2 × 2
multiple-input and multiple-output (MIMO) frequency-domain equalizer. The feasibility
of the proposed PM-DMT-DD system and the effectiveness of the novel DSP algorithms
are investigated via theoretical and simulation studies.

Index Terms: Polarization-multiplexing, intensity modulation and direct-detection, discrete
multi-tone.

1. Introduction

The rapid growth of Internet traffic has incessantly driven the bandwidth demand for optical
networks. Based on the use of powerful digital signal processing and coherent detection, long-
haul optical transmission has experienced rapid capacity improvement in recent years [1], [2].
However, different from long-haul networks, short-reach applications are much more sensitive
to the cost of transceivers. Comparing with coherent detection, the cost-efficient intensity modu-
lation with direct detection (IM-DD) is more attractive for short reach transmission systems [3].
In order to increase single wavelength transmission rate by using low cost optical components
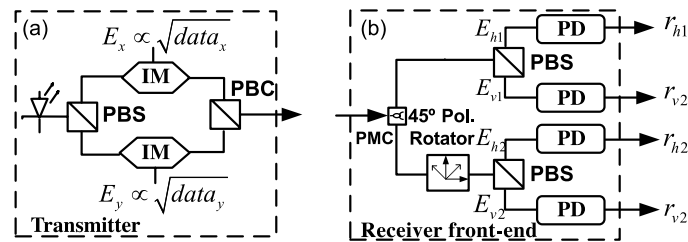
Fig. 1. (a) Transmitter and (b) receiver front-end structure for the proposed PM-DMT-DD system. IM: intensity modulator, PBS: polarization beam splitter, PBC: polarization beam combiner, PD: photo-detector, PMC: polarization maintaining coupler.

with limited bandwidth, a number of advanced modulation formats combined with IM-DD have been investigated to achieve high spectral efficiency, including pulse amplitude modulation (PAM) [4], [5], carrier-less amplitude and phase modulation (CAP) [6], [7], and discrete multi-tone (DMT) [8], [9].

Recently, polarization multiplexing with DD has been studied to further increase data rate. D. Qian *et al.* first proposed the use of PM with IM-DD in short reach transmission based on single sideband orthogonal frequency division multiplexing (SSB-OFDM) modulation [10]. However, this PM-OFDM-DD system requires a complex transmitter structure involving RF source and narrow-band optical filters. Furthermore, the primary problem associated with the proposed scheme is that the singularity of its 4×4 transfer matrix will lead to a failure of the polarization de-multiplexing scheme when the received state of polarizations (SOP) is at $\pm \pi/4$ and integer multiples of this value to the axis of the receiver polarization beam splitter (PBS). Over the past two years, PM combined with Stokes-based DD reception has been proposed as a new approach to increase the bit rate in a single wavelength channel, including PM with PAM [11], [12] and signal-carrier PM with OFDM [13]. Here, the singularity problem in the transfer matrix can be avoided. In the proposed schemes [11], [13], Stokes Vectors are required to be obtained by using a 90° hybrid with balanced detections. In [12], Stokes Vectors can be obtained in DSP based on a blind SOP tracking feedback algorithm. However, this scheme is only suitable for binary baseband modulation on two orthogonal polarizations. In addition to above endeavors, the latest work in [14] proposed a quaternary polarization multiplexed system to support four independent non-return-to-zero OOK signals transmission in four different SOPs and realized 108 and 128 Gb/s experimental 2 km SSMF transmission in 1550 nm.

In our previous work in [15], a polarization-interleave-multiplexed discrete multi-tone (PIM-DMT) system was proposed, in which two lasers with different frequencies are required for two polarizations, and their frequency difference should be larger than signal bandwidth so as to remove the influence of the mixed polarization beat interference (MPBI). In this paper, we improve the work of [15] and propose a novel PM-DMT-DD system, where one laser source is used without the frequency spacing, and a simple receiver structure is employed without 90° hybrid and balanced detections. Based on the new SOP estimation and MPBI elimination algorithms, the influence of MPBI can be removed in the digital domain in the proposed system. After this, polarizations de-multiplexing and channel estimation can be realized by using the traditional 2×2 MIMO equalizer in the frequency domain. Finally, the feasibility of the proposed PM-DMT-DD system and the effectiveness of the corresponding DSP algorithms are demonstrated through simulation.

2. Operation Principle

The block diagrams of the transmitter and receiver front-end structure of the proposed PM-DMT-DD system are shown in Fig. 1. At the transmitter side, two real value DMT signals are modulated onto the intensity of two orthogonal polarizations of one laser, and transmitted after a polarization beam combiner (PBC). After propagation through an optical fiber, the

intensity modulated PM-DMT signal is divided into two different SOPs, which are with a fixed $\pi/4$ polar angle difference, as shown in Fig. 1(b).

It is well known that the frequency-selective fading will be induced by fiber dispersion in IM-DD systems. In order to avoid this effect, short reach systems commonly use the zero-chromatic-dispersion (CD) wavelength in the O-band of SMF around 1310 nm. Besides, because of the short transmission distance ($\leqslant$ 80 km), polarization mode dispersion (PMD) is very small. In this case, we only consider a random polarization rotation in following theoretical derivations for simplicity. (However, PMD tolerance will be evaluated through simulation for the proposed system in Section 3, so as to demonstrate the robustness of the PM-DMT-DD system in the presence of PMD.) Then, the received electric fields of the PM-DMT signals in two SOPs, i.e., $E_{h1(2)}$, $E_{v1(2)}$, can be written as

$$\begin{bmatrix} E_{h1(2)}(t) \\ E_{v1(2)}(t) \end{bmatrix} = R_{1(2)} \cdot \begin{bmatrix} E_x(t) \\ E_y(t) \end{bmatrix} \tag{1}$$

where E_x, E_y denote the two field components of the horizontal and vertical polarizations in the transmitter, respectively, $R_{1(2)}$ are channel rotation matrixes

$$R_1 = \begin{pmatrix} \cos\theta_1 e^{j\varepsilon/2} & -\sin\theta_1 e^{-j\varepsilon/2} \\ \sin\theta_1 e^{j\varepsilon/2} & \cos\theta_1 e^{-j\varepsilon/2} \end{pmatrix} \tag{2}$$

$$R_2 = R_1 \cdot \begin{pmatrix} \cos\pi/4 & -\sin\pi/4 \\ \sin\pi/4 & \cos\pi/4 \end{pmatrix} = \begin{pmatrix} \cos\theta_2 e^{j\varepsilon/2} & -\sin\theta_2 e^{-j\varepsilon/2} \\ \sin\theta_2 e^{j\varepsilon/2} & \cos\theta_2 e^{-j\varepsilon/2} \end{pmatrix}_{\theta_2 = \theta_1 + \frac{\pi}{4}} \tag{3}$$

where θ_1 and θ_2 denote the random polar angles for the two received SOPs, respectively, which have a fixed $\pi/4$ difference, and ε is the random azimuth angle.

Then four square-law PDs are employed to realize optical-to-electrical (O/E) conversion for E_{h1}, E_{v1}, E_{h2}, and E_{v2}, respectively. After sampling by analog to digital converters (ADCs), the kth received samples can be expressed as

$$r_{h1(2)}(k) = \left|E_{h1(2)}(k)\right|^2 + w_{h1(2)}(k) = \cos^2\theta_{1(2)}|E_x(k)|^2 + \sin^2\theta_{1(2)}\left|E_y(k)\right|^2$$
$$- 2\cos\theta_{1(2)}\sin\theta_{1(2)}\mathrm{Re}\left\{E_x(k)E_y^*(k)e^{-j\varepsilon}\right\} + w_{h1(2)}(k) \tag{4}$$

$$r_{v1(2)}(k) = \left|E_{v1(2)}(k)\right|^2 + w_{v1(2)}(k) = \sin^2\theta_{1(2)}|E_x(k)|^2 + \cos^2\theta_{1(2)}\left|E_y(k)\right|^2$$
$$+ 2\cos\theta_{1(2)}\sin\theta_{1(2)}\mathrm{Re}\left\{E_x(k)E_y^*(k)e^{j\varepsilon}\right\} + w_{v1(2)}(k) \tag{5}$$

where $\mathrm{Re}\{\}$ denotes the real part of a complex number, $(.)^*$ denotes the complex conjugate, and w is Gaussian white noise (AWGN). The photodiode responsivity is assumed as 1. Due to intensity modulation, $E_x(k)E_y^*(k)$ is a real number. Therefore, (4) and (5) can be further simplified as

$$r_{h1(2)}(k) = \cos^2\theta_{1(2)}|E_x(k)|^2 + \sin^2\theta_{1(2)}\left|E_y(k)\right|^2 - 2\cos\theta_{1(2)}\sin\theta_{1(2)}\cos\varepsilon E_x(k)E_y^*(k) + w_{h1(2)}(k) \tag{6}$$

$$r_{v1(2)}(k) = \sin^2\theta_{1(2)}|E_x(k)|^2 + \cos^2\theta_{1(2)}\left|E_y(k)\right|^2 + 2\cos\theta_{1(2)}\sin\theta_{1(2)}\cos\varepsilon E_x(k)E_y^*(k) + w_{v1(2)}(k). \tag{7}$$

From (6) and (7), we can see that the first two terms of them contain the transmitted signals in the X and Y polarization respectively, but the third term is an undesirable product, i.e., MPBI. Being different from our previous work [15], there is no frequency difference between E_x and E_y to remove the mixing product. It is known that due to the mechanical and temperature fluctuation, optical channel usually varies on the time scale of a millisecond in practice [16]. Based on the slow-varying characteristic of optical channel, channel impairments can be assumed as constant within a signal processing frame. Taking the training-symbols-based frame design as traditional OFDM systems [16], [17], a simple SOP estimation algorithm is proposed to calculate SOP periodically, and the influence of MPBI can be removed in DSP based on the SOP estimation result.
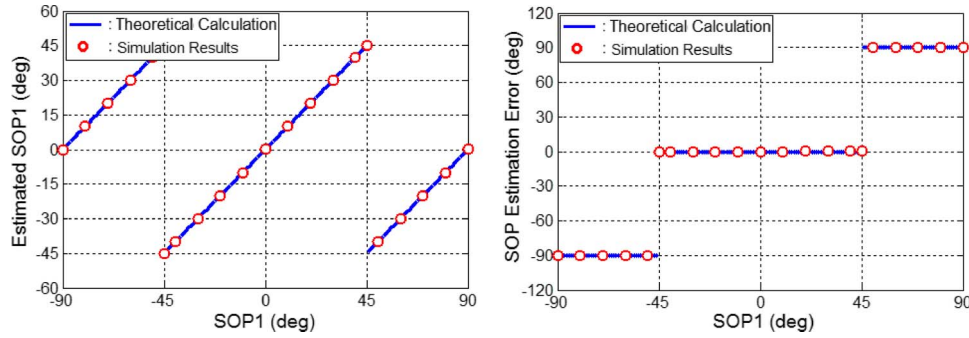
Fig. 2. (a) $\hat{\theta}_1$ and (b) the estimation error as a function of the different SOP1.

2.1 SOP Estimation

At the beginning of each estimation period, n training data are loaded on both orthogonal polarizations simultaneously, where $|E_y(k)|^2 = |E_x(k)|^2$, $k \in [1, n]$. In DMT, the training data for frame synchronization can be designed and reused for the SOP estimation to avoid extra training overhead. Here, the kth received samples of $r_{h1(2)}$ and $r_{v1(2)}$ can be expressed as

$$r_{h1(2)}(k) = |E_x(k)|^2 - 2\cos\theta_{1(2)}\sin\theta_{1(2)}\cos\varepsilon|E_x(k)|^2 + w_{h1(2)}(k) \tag{8}$$

$$r_{v1(2)}(k) = |E_x(k)|^2 + 2\cos\theta_{1(2)}\sin\theta_{1(2)}\cos\varepsilon|E_x(k)|^2 + w_{v1(2)}(k). \tag{9}$$

Then, the polarization-related impairments can be estimated from (8) and (9) by using these n training samples, as

$$d_{1(2)} = \frac{\sum_n r_{v1(2)} - \sum_n r_{h1(2)}}{\sum_n r_{h1(2)} + \sum_n r_{v1(2)}} \approx 2\cos\theta_{1(2)}\sin\theta_{1(2)}\cos\varepsilon = \sin(2\theta_{1(2)})\cos\varepsilon \tag{10}$$

where $\sum(.)$ denotes the sum operation, that is used to suppress AWGN effect, n is the number of training samples. Next, the azimuth angle ε-induced product can be removed by

$$\frac{d_1}{d_2} \approx \frac{\sin(2\theta_1)}{\sin(2\theta_2)} = \frac{\sin(2\theta_1)}{\sin\left(2\theta_1 + \frac{\pi}{2}\right)} = \frac{\sin(2\theta_1)}{\cos(2\theta_1)} = \tan(2\theta_1). \tag{11}$$

According to (11), without a convergence process as in [12], the SOP can be easily estimated in a feed-forward manner as

$$\hat{\theta}_1 = \frac{1}{2}\arctan\left(\frac{d_1}{d_2}\right) \tag{12}$$

where $\arctan(.)$ denotes the inverse tangent operation. Then, $\hat{\theta}_2$ can be obtained by $\hat{\theta}_1 + \pi/4$ based on their fixed polar-angle difference relationship.

To validate the correctness of the SOP estimation algorithm, the results obtained by theoretical calculation and simulation conducted on the PM-DMT-DD system by using 128 training samples in the back-to-back (BTB) scenario (the detailed system description can be found in Section 3) are depicted together in Fig. 2(a). It can be seen that the simulation results agree well with the theoretical results as expected. However, due to the results of $\arctan(.)$ are limited in the range of $[-\pi/2, \pi/2]$, $\hat{\theta}_1$ will be kept within $[-\pi/4, \pi/4]$. Here, the inherent angle ambiguity may cause $\pm\pi/2$-based estimation error (see Fig. 2(b)), and the final estimation results can be represented as

$$\hat{\theta}_{1(2)} = \theta_{1(2)} \pm l \cdot \pi/2 + \Delta e, \quad l = 0, 1, 2\ldots \tag{13}$$

where Δe is called the effective SOP estimation error, and $l \cdot \pi/2$ denotes the $\pi/2$-based angle ambiguity, which will be proved to have no effects on the proposed system in the next sub-section.

2.2 MPBI Elimination

After the SOP estimation, the MPBI-induced products, i.e., the 3rd term of Eq. (6) and (7), will be removed by using $\hat{\theta}_1$ and $\hat{\theta}_2$. Here, two MPBI elimination schemes are given as follows:

For scheme 1, a new pair of received signal r'_h and r'_v without MPBI can be calculated as

$$r'_{h(v)}(k) = r_{h1(v1)}(k) - r_{h2(v2)}(k) \cdot \frac{\cos\hat{\theta}_1 \sin\hat{\theta}_1}{\cos\hat{\theta}_2 \sin\hat{\theta}_2}. \tag{14}$$

Assuming that $\Delta e = 0$ in (13) and substituting $\hat{\theta}_{1(2)} = \theta_{1(2)} \pm l \cdot \pi/2$ into (14), we can obtain

$$
\begin{aligned}
r'_{h(v)}(k) &= r_{h1(v1)}(k) - r_{h2(v2)}(k) \cdot \frac{\cos(\theta_1 \pm l \cdot \pi/2)\sin(\theta_1 \pm l \cdot \pi/2)}{\cos(\theta_2 \pm l \cdot \pi/2)\sin(\theta_2 \pm l \cdot \pi/2)} \\
&= r_{h1(v1)}(k) - r_{h2(v2)}(k) \cdot \frac{\cos\theta_1 \sin\theta_1}{\cos\theta_2 \sin\theta_2}.
\end{aligned}
\tag{15}
$$

From (15), it can be found that the $\pm\pi/2$-based estimation ambiguity has no effect on MPBI elimination. Next, we substitute (6) and (7) into (15), r'_h and r'_v can be further given by

$$
\begin{bmatrix} r'_h(k) \\ r'_v(k) \end{bmatrix} = R' \begin{bmatrix} |E_x(k)|^2 \\ |E_y(k)|^2 \end{bmatrix} + \begin{bmatrix} w'_h(k) \\ w'_v(k) \end{bmatrix}
\tag{16}
$$

where R' is the new polarization rotation matrix for scheme 1

$$
R' = \begin{bmatrix} \frac{\cos\theta_1}{\sin\theta_1 + \cos\theta_1} & \frac{-\sin\theta_1}{\cos\theta_1 - \sin\theta_1} \\ \frac{-\sin\theta_1}{\cos\theta_1 - \sin\theta_1} & \frac{\cos\theta_1}{\sin\theta_1 + \cos\theta_1} \end{bmatrix}
\tag{17}
$$

and w'_h and w'_v denote the altered noise terms, i.e.,

$$w'_h(k) = w_{h1}(k) - w_{h2}(k)\tan(2\theta_1), \quad w'_v(k) = w_{v1}(k) - w_{v2}(k)\tan(2\theta_1). \tag{18}$$

Note that θ_2 has been replaced by $\theta_1 + \pi/4$ and simplified in (17) and (18), and the influence of ε has been cancelled with MBPI during the subtraction process of (15).

For scheme 2, another pair of received signal r''_h and r''_v without MPBI can be calculated as

$$r''_{h(v)}(k) = r_{v1(h1)}(k) + r_{h2(v2)}(k) \cdot \frac{\cos\hat{\theta}_1 \sin\hat{\theta}_1}{\cos\hat{\theta}_2 \sin\hat{\theta}_2}. \tag{19}$$

Similarly, r''_h and r''_v can be obtained by

$$
\begin{bmatrix} r''_h(k) \\ r''_v(k) \end{bmatrix} = R'' \begin{bmatrix} |E_x(k)|^2 \\ |E_y(k)|^2 \end{bmatrix} + \begin{bmatrix} w''_h(k) \\ w''_v(k) \end{bmatrix}
\tag{20}
$$

where R'' is the polarization rotation matrix for r''_h and r''_v,

$$
R'' = \begin{bmatrix} \frac{\sin\theta_1}{\sin\theta_1 + \cos\theta_1} & \frac{\cos\theta_1}{\cos\theta_1 - \sin\theta_1} \\ \frac{\cos\theta_1}{\cos\theta_1 - \sin\theta_1} & \frac{\sin\theta_1}{\sin\theta_1 + \cos\theta_1} \end{bmatrix}
\tag{21}
$$

and

$$w''_h(k) = w_{v1}(k) + w_{h2}(k)\tan(2\theta_1), \quad w''_v(k) = w_{h1}(k) + w_{v2}(k)\tan(2\theta_1). \tag{22}$$

From (18) and (22), it can be seen that the noise will be changed with the received SOP. It is necessary to take the noise effects into account to analyze the process of polarization de-multiplexing and decide a suitable scheme choice from above two MBPI elimination schemes.

2.3 Polarization De-Multiplexing

As one of OFDM systems, the proposed PM-DMT-DD system can use the traditional 2×2 MIMO frequency-domain equalizer to de-multiplex polarization after MBPI elimination. For simplicity, we assume the output signal of the Fast Fourier Transform (FFT) operation in a more concise form as

$$\begin{bmatrix} R_{H,i} \\ R_{V,i} \end{bmatrix} = \underbrace{\begin{bmatrix} A_i & B_i \\ C_i & D_i \end{bmatrix}}_{\text{ChannelMatrix } H_i} \begin{bmatrix} X_i \\ Y_i \end{bmatrix} + \begin{bmatrix} N_{H,i} \\ N_{V,i} \end{bmatrix} \tag{23}$$

where the subscript i denotes the index of subcarrier, H_i is the channel matrix, X_i and Y_i represent the transmitted data in the ith subcarrier for X-pol and Y-pol respectively, $N_{H(V)}$ denotes the random noise. Note that the index of DMT symbol sequence is ignored here for explanatory simplicity.

Then, the channel matrix H_i can be easily estimated based on the time-interleaved training symbols (the detailed description can be found in [15]). Once the channel transfer matrix H_i are known and combined with the received signal R_H and R_V, the estimated transmitted symbols $\hat{X}_i$ and $\hat{Y}_i$ will be readily computed as follows:

$$\begin{bmatrix} \hat{X}_i \\ \hat{Y}_i \end{bmatrix} = H_i^{-1} \begin{bmatrix} R_{H,i} \\ R_{V,i} \end{bmatrix} = \begin{bmatrix} X_i \\ Y_i \end{bmatrix} + \begin{bmatrix} N'_{H,i} \\ N'_{V,i} \end{bmatrix} \tag{24}$$

where $(.)^{-1}$ denotes the inverse of the matrix, and

$$N'_{H,i} = \frac{D_i N_{H,i} - B_i N_{V,i}}{A_i D_i - C_i B_i}, \ N'_{V,i} = \frac{A_i N_{V,i} - C_i N_{H,i}}{A_i D_i - C_i B_i}. \tag{25}$$

Now, consider analytically the effects of $N'_{H,i}$ and $N'_{V,i}$ when using above two MBPI elimination schemes. Here, we omit the dispersion-related influences. In this case, the H_k can be replaced by R' and R''. Taking scheme 1 as an example

$$A_i = D_i = \frac{\cos\theta_1}{\sin\theta_1 + \cos\theta_1}, \ B_i = C_i = \frac{-\sin\theta_1}{\cos\theta_1 - \sin\theta_1} \tag{26}$$

and $N_{H,i}$ and $N_{V,i}$ can be obtained as

$$N_{H,i} = W_{H1,i} - W_{H2,i}\tan(2\theta_1), \ N_{V,i} = W_{V1,i} - W_{V2,i}\tan(2\theta_1) \tag{27}$$

where $W_{H1,V1,H2,V2}$ is $w_{h1,v1,h1,v2}$ after the FFT operation, which still maintain AWGN characteristics. Next, substituting (26) and (27) into (25), we can quantitatively analyze the variation of noise power with θ_1 for the scheme 1. Fig. 3 shows the average noise power as a function of the received SOP1. Here, in order to focus on the change, the average noise power is normalized with respect to its value at SOP1 $= 0$ and measured in decibels.

Similarly, the noise power change versus SOP1 by using scheme 2 can also be analyzed, and the theoretical calculation results are depicted in Fig. 3 with red circular marks. It can be seen that there is no one-size-fits-all approach. Due to the matrix singularity problem of R' and R'', noise is amplified periodically, and the maximum impairment will occur at SOP1 $= -\pi/8 \pm I \cdot \pi/2$ ($I = 0, 1, 2 \ldots$) for scheme 1, and at SOP1 $= \pi/8 \pm I \cdot \pi/2$ for scheme 2, respectively. However, the two schemes are exactly complementary. In order to avoid signal-noise ratio (SNR) deterioration, the two MBPI elimination schemes can be selected based on the estimation result of SOP1 $- \hat{\theta}_1$, i.e. if $\hat{\theta}_1 \in (0, \pi/4]$, scheme 1 will be chosen; else, if $\hat{\theta}_1 \in$
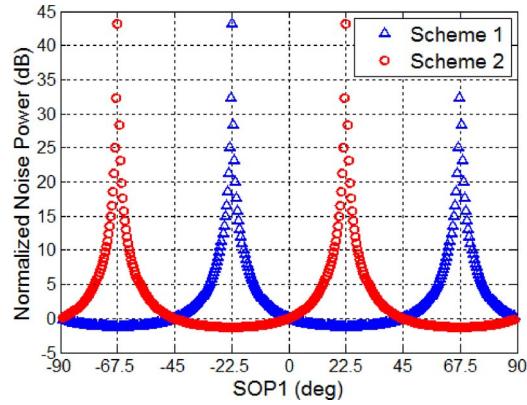
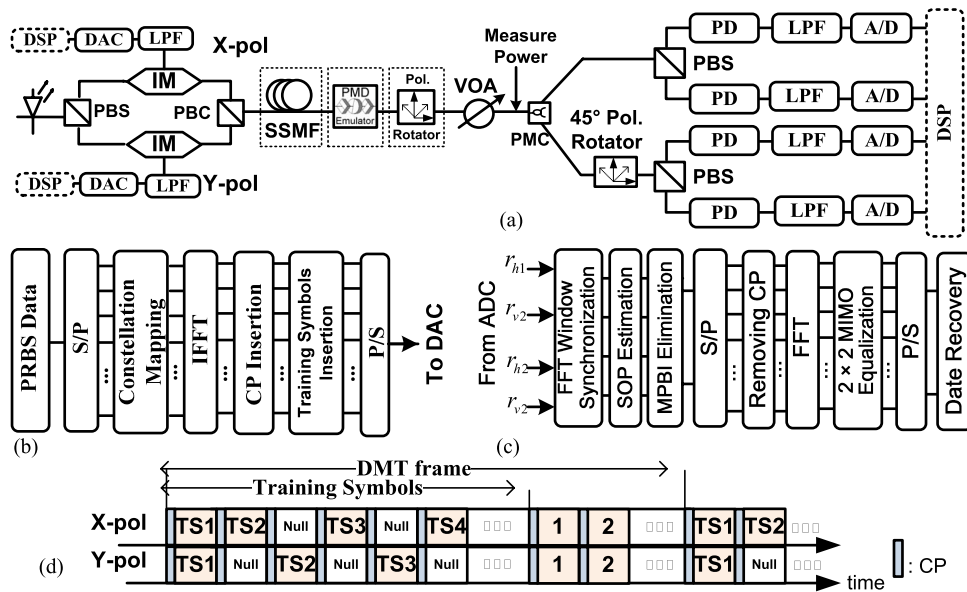Fig. 3. Normalized noise power as a function of the received SOP.

Fig. 4. (a) Simulation setup of PM-DMT-DD system, the schematics of the DSP in the transmitter (b) and receiver (c), and (d) DMT frame structure. SSMF: standard single mode fiber; VOA: variable optical attenuator.

$[-\pi/4, 0]$, scheme 2 will be chosen. Here, the $\pi/2$-based angle ambiguity problem of $\hat{\theta}_1$ has also no effect on the scheme decision, because the noise power change also follows with the same $\pi/2$-based period. From Fig. 3, it still can be found that the best SNR can be obtained at SOP1 $= \pi/8 \pm l \cdot \pi/4$ instead of SOP1 $= 0$. So, the average SNR will be slightly better than that of SOP1 $= 0$ in theory.

3. Simulation and Discussion

3.1 Simulation Model

The simulation model for the proposed PM-DMT-DD system is built by VPI transmission Maker 8.7 and MATLAB software, as shown in Fig. 4(a). At the transmitter, DSP modules are performed to generate the DMT baseband signals. The different signal processing steps for one polarization are shown in Fig. 4(b). The pseudo-random bit sequence (PRBS) with a length of $2^{17} - 1$ as the transmitted data stream is mapped into 16 QAM. Then, the time domain DMT

TABLE 1

General simulation parameters

Parameter	Values	Parameter	Values
Modulation format (w/o variable bit loading)	16QAM	Laser RIN	-160dB/Hz
IFFT/FFT size	128	Laser line-width	5MHz
Number of Data Subcarriers	56	PD responsibility	0.65 A/W
DAC/ADC rate	64GSam/s	PD thermal noise	$20pA/Hz^{0.5}$
TX/RX 3dB-bandwidth	20GHz	PD dark current	10nA

symbol is generated by an IFFT of size 128. To satisfy the Hermitian symmetry property of DMT, there are 56 subcarriers in positive frequency loaded with the encoded data, 56 symmetric subcarriers in negative frequency loaded with their conjugate data, and the rest of null subcarriers retained for dc-bias and oversampling. To counter fiber dispersion-induced inter-symbol interference (ISI), cyclic prefix (CP) is added to each of DMT symbol. Here, CP is set to be 10 to guarantee a sufficient margin for ISI effects in all the simulations, which can be further optimized in practice.

Subsequently, 41 training symbols are inserted at the beginning of each DMT frame, as illustrated in Fig. 4(d), which consist of one training symbol for symbol synchronization and SOP estimation, and 40 time-interleaved training symbols for channel estimation (including 20 null symbols that are located in odd/even time slots in X/Y-pol respectively). Here, the time of one DMT frame is set to be 4.3 μs (corresponding to 2000 DMT symbols in our system), which is fast enough to track the change of optical channel, since the optical channel usually varies on the time scale of a millisecond due to the mechanical and temperature fluctuation [16]. And then, the digital DMT signals are uploaded into DAC operated at 64 GSam/s with 8 bits resolution, and filtered by fourth-order Bessel low pass filter (LPF) so as to simulate the bandwidth limitation of transmitter. After filtering, the signals are modulated onto the intensity of two orthogonal polarizations from an optical laser at 1310 nm to avoid the CD-induced frequency selective fading. After a PBC, the PM-DMT-DD signal is obtained with $\sim$204 Gb/s ($= 64$ GSam/s $* 8 * 56/138 * (2000 - 41)/2000$) data rate without considering the FEC overhead.

The transmission link compose of standard single mode fiber (SSMF), a PMD emulator (PMD-E) that is used to impose arbitrary different group delay (DGD) to signal, a polarization rotator (PR) that is used to change received SOP, and a variable optical attenuator (VOA) that is used to adjust the received optical power. Noted that the devices in the dotted box can be switched independently, and PMD-E and PR are mainly used in the BTB cases. At the receiver, the PM-DMT signal is detected in two SOPs with $\pi/4$ polar-angle difference by utilizing four photodiodes (PDs), as depicted in Fig. 4(a). Next, the electrical signals were digitized by ADCs at 64 GSam/s with 8-bit of resolution and stored for DSP using MATLAB, as shown in Fig. 4(c). Table 1 summarizes the general settings of the simulation parameters.

3.2 Simulation Results and Analysis

First of all, the accuracy of SOP estimation as a function of the number of training samples is investigated in BTB transmissions with different receiver optical powers. Because the $\pm\pi/2$-based inherent error has no effect on the result, we only focus on the effective SOP estimation error—Δe (see (13)). Here, the polarization rotation angle θ_1 and the azimuth angle ε are changed randomly for each simulation, and more than 400 sets of date are run for each measurement point. As shown in Fig. 5, the estimation accuracy can be improved with the increasing number of training samples. Based on the proposed SOP estimation algorithm, $|\Delta e|$ can be readily kept within 1 degree. For 128 training samples, there is only about 0.1° SOP estimation error. The effect of residual estimation error can be ignored.
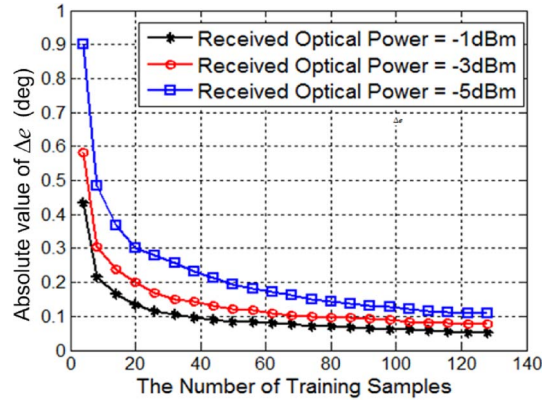
Fig. 5. Absolute value of $\triangle e$ as a function of the number of training data in BTB transmissions.
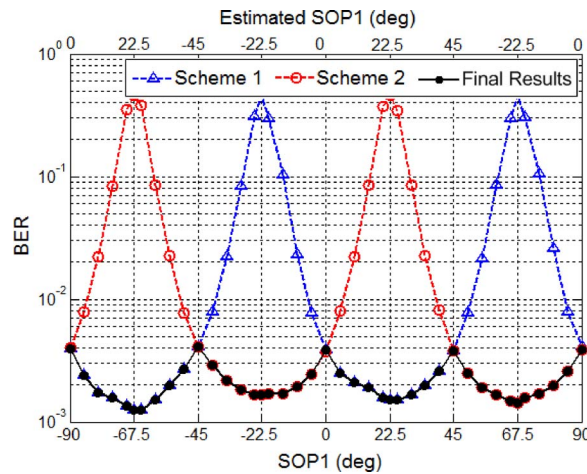

Fig. 6. Measured BER as a function of SOPs in BTB transmissions (received optical power $= -3$ dBm).

In order to avoid the singularity problem of the transfer matrix, two MBPI elimination schemes have to be selected after SOP estimation. This theoretical result is further validated by the simulation. Fig. 6 shows the BERs obtained by three approaches at different received SOPs. It can be seen that the BER performances get worse obviously while SOP1 is located at $[-\pi/4,\ 0] \pm l \cdot \pi/2$ by using scheme 1, but the use of scheme 2 causes the BER deterioration while SOP1 at $[0,\ \pi/4] \pm l \cdot \pi/2$, and the worst-case results occur at SOP1 $= -\pi/8 \pm l \cdot \pi/2$ and SOP1 $= \pi/8 \pm l \cdot \pi/2$ for the two schemes respectively as expected. Moreover, better BER results are obtained for SOP1 $= \pi/8 \pm l \cdot \pi/4$ instead of SOP1 $= \pm l \cdot \pi/4$, which are in agreement with the theoretical noise power change as shown in Fig. 3. According to the $\hat{\theta}_1$-based scheme selection rule (namely, if $\hat{\theta}_1 \in (0, \pi/4]$, scheme 1 will be chosen; else, if $\hat{\theta}_1 \in [-\pi/4, 0]$, scheme 2 will be chosen), the final BERs are measured and plotted with black solid line in Fig. 6. These results demonstrate the feasibility of this selection approach.

Fig. 7 depicts the BER as a function of the received optical power for SOP1 at 0 and $\pi/8$ in BTB transmissions. Here, the BER measured by two single polarization (SP) DMT-DD in different wavelength channels with total 204 Gb/s data rate is also shown as a reference. For a fair comparison, the same simulation parameters listed in Table 1 are also used for the two SP-DMT-DD systems. It can be seen that at the same bit rate, the difference in received optical power between 2×SP-DMT-DD and PM-DMT-DD at SOP1 $= 0$ is about 3 dB. Since during SOP1 $= 0$, r_{v1} and r_{v2} will be remained after MBPI elimination (see Fig. 1(b)), and the received optical power
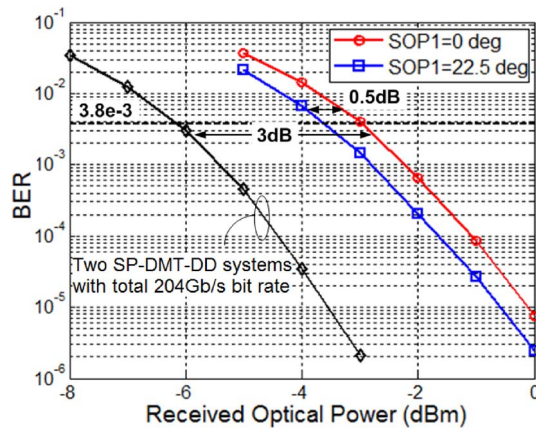
Fig. 7. Measured BER as a function of the received optical power in BTB transmissions.
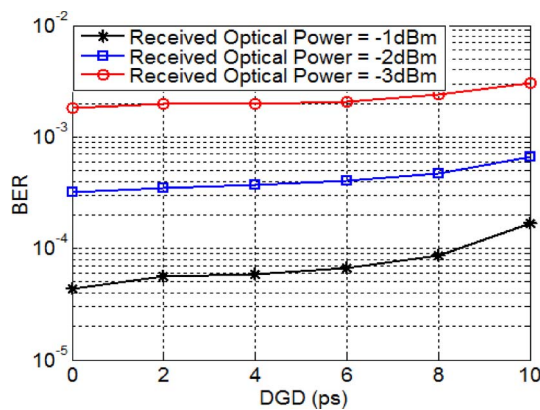

Fig. 8. Measured BER as a function of DGD for different received optical power.

is halved to input to these two PDs, 3-dB higher received power is required for PM-DMT-DD system to obtain a same SNR in comparison to 2×SP-DMT-DD under the thermal noise-dominated scenario. It can also be seen from Fig. 7 that the received power requirement can be slightly reduced (~0.5 dB) for SOP1 = $\pi/8$ resulting from the decreasing noise contribution after polarization de-multiplexing.

In the presence of random fiber birefringence, the SOP is only rotated and both polarization modes remain orthogonal to each other. However, due to PMD, the coupling between the polarization modes will generally result in a transmission impairment for the polarization multiplexed signal. Over short transmission distance at 1310 nm wavelength region, PMD is small but still exists. Therefore, the PMD tolerance is here studied for our proposed PM-DMT-DD system. A PMD emulator is added before the receiver to impose arbitrary DGD to signal. Fig. 8 depicts BER as a function of the DGD with the different received optical power by using the proposed PM-DMT-DD system. Here, the maximum 10 ps DGD is considered, since modern optical fiber can have a low PMD parameter in the order of 0.05 ps/$\sqrt{\text{km}}$ [18]. A 10 ps DGD can correspond to a SSMF transmission distance over hundreds of kilometers by considering the instant maximum DGD 3.7 times larger than the mean DGD (i.e., PMD), which far exceeds the requirement of PMD tolerance for the short-reach applications. From Fig. 8, it can be seen that only a small BER reduction caused by the increase of DGD. Up to 10 ps of DGD, the received optical power penalty can be less than 0.5 dB. These results demonstrate the feasibility of our proposed algorithms and the robustness of the PM-DMT-DD system in the presence of PMD.
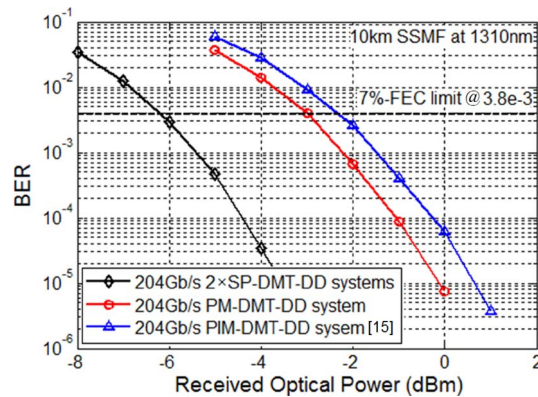
Fig. 9. BER as a function of received optical power after 10 km SSMF transmission.

Fig. 9 depicts BER performance as a function of received power after 10 km SSMF transmission. Here, the PMD parameter of fiber is set to be 0.1 ps/$\sqrt{}$km. The results using our previous proposed PIM-DMT-DD system [15] and two SP-DMT-DD systems with total 204 Gb/s bit rate are also displayed in Fig. 9 for comparison, where the same simulation parameters as shown in Table 1 are also adopted for these two systems. Besides, in the term of the PIM-DMT-DD system, a frequency spacing of 96 GHz between two polarizations is used in order to avoid the beating interference. First, comparing the two dual-polarizations systems, the better performance can be achieved by using the PM-DMT-DD system. These two dual-polarizations systems have the same receiver structure, and can achieve same performance at SOP1 = 0 in theory. However, SOP1 = 0 is the worst case for PM-DMT-DD system (see Fig. 6) but the best case for PIM-DMT-DD system [15, Fig. 8(b)], which results in the difference in average performance between them. Next, it can be seen that the difference in received optical power requirement between 204 Gb/s DMT-DD with polarization multiplexing and multi-channels is about 3 dB for a 3.8×10^{-3} BER, which generally stems from four PDs employed in the proposed PM-DMT-DD system contribute 3-dB higher amount of thermal noise in comparison to two PDs used for two single polarization DMT-DD systems. However, in comparison to other existing PM-DD schemes, such as [11], [13], the proposed PM-DMT-DD system has a much simpler receiver structure. On the other hand, if we choose to use higher order modulation instead polarization multiplexing to upgrade the transmission rate up to 200 Gb/s, 256-QAM has to be used (it can be seen as a average modulation level that should to be achieved after using bit-loading in DMT), which requires a ~8.5 dB higher E_b/N_0 (the energy per information bit-to-noise spectral density ratio) than 16 QAM at a BER of 3.8e-3 in theory [19] without considering other implementation limitations, such as the effective number of bits (ENOB) of ADC/DAC. As a result, the proposed PM-DMT-DD system should be a low-cost solution for increasing the transmission capacity for every single LAN-WDM channel.

4. Conclusion

In this paper, a novel PM-DMT system with IM-DD is proposed, which can double the maximum achievable bit rate for a single wavelength channel with a simple transmitter and receiver structure. Moreover, the corresponding DSP algorithms, i.e., SOP estimation and MPBI elimination, have also been proposed to achieve optimized system performance in the presence of random polarization crosstalk. Simulation results show that based on a small number of training symbols, high accuracy SOP estimation can be guaranteed without a convergence process, and after MPBI elimination, the traditional 2 × 2 MIMO equalizer is able to realize polarization de-multiplexing and achieve high PMD tolerance. The new PM-DMT-DD transceiver may be a promising cost-efficient solution for future short reach optical transmission system to upgrade to 200 Gbit/s and beyond in a single wavelength channel.

References

[1] X. Liu, S. Chandrasekhar, and P. J. Winzer, "Digital signal processing techniques enabling multi-Tb/s superchannel transmission: An overview of recent advances in DSP-enabled superchannels," *IEEE Signal Process. Mag.*, vol. 31, no. 2, pp. 16–24, Mar. 2014.

[2] A. P. T. Lau *et al.*, "Advanced DSP techniques enabling high spectral efficiency and flexible transmissions: Toward elastic optical networks," *IEEE Signal Process. Mag.*, vol. 31, no. 2, pp. 82–92, Mar. 2014.

[3] K. P. Zhong *et al.*, "Experimental study of PAM-4, CAP-16, and DMT for 100 Gb/s short reach optical transmission systems," *Opt. Exp.*, vol. 32, no. 2, pp. 1176–1189, Jan. 2015.

[4] M. Chagnon *et al.*, "Experimental study of 112 Gb/s short reach transmission employing PAM formats and SiP intensity modulator at 1.3 μm," *Opt. Exp.*, vol. 22, no. 17, pp. 21018–21036, Aug. 2014.

[5] K. P. Zhong *et al.*, "140 Gbit/s 20 km transmission of PAM-4 signal at 1.3 μm for short reach communications," *IEEE Photon. Technol. Lett.*, vol. 27, no. 16, pp. 1757–1760, Aug. 2015.

[6] M. I. Olmedo *et al.*, "Multiband carrierless amplitude phase modulation for high capacity optical data links," *J. Lightw. Technol.*, vol. 32, no. 4, pp. 798–804, Feb. 2014.

[7] L. Tao *et al.*, "Experimental demonstration of 10 Gb/s multi-level carrier-less amplitude and phase modulation for short range optical communication systems," *Opt. Exp.*, vol. 21, no. 5, pp. 6459–6465, Mar. 2013.

[8] F. Li, X. Li, J. Yu, and L. Chen, "Optimization of training sequence for DFT-spread DMT signal in optical access network with direct detection utilizing DML," *Opt. Exp.*, vol. 22, no. 19, pp. 22962–22967, Sep. 2014.

[9] K. Takabayashi and J. C. Rasmussen, "Experimental demonstration of 448-Gbps+ DMT transmission over 30 km SMF," presented at the Opt. Fiber Commun. Conf., San Francisco, CA, USA, 2014, Paper M2I.5.

[10] D. Qian, N. Cvijetic, J. Hu, and T. Wang, "108 Gb/s OFDMA-PON with polarization multiplexing and direct detection," *J. Lightw. Technol.*, vol. 28, no. 4, pp. 484–493, Feb. 2010.

[11] M. Morsy-Osman, M. Chagnon, M. Poulin, S. Lessard, and D. V. Plant, "1$\lambda \times$ 224 Gb/s 10 km transmission of polarization division multiplexed PAM-Signals using 1.3 μm SiP intensity modulator and a direct-detection MIMO-based receiver," presented at the Eur. Conf. Opt. Commun., Cannes, France, 2014, Paper PD. 4.4.

[12] K. Kikuchi, "Electronic polarization-division demultiplexing based on digital signal processing in intensity-modulation direct-detection optical communication systems," *Opt. Exp.*, vol. 22, no. 2, pp. 1971–1980, Jan. 2014.

[13] D. Che *et al.*, "Stokes vector direct detection for linear complex optical channels," *J. Lightw. Technol.*, vol. 33, no. 3, pp. 678–684, Feb. 2015.

[14] J. Estarán *et al.*, "Quaternary polarization-multiplexed subsystem for high-capacity IM/DD optical data links," *J. Lightw. Technol.*, vol. 33, no. 7, pp. 1408–1416, Apr. 2015.

[15] X. Zhou *et al.*, "Polarization-interleave-multiplexed discrete multi-tone modulation with direct detection utilizing MIMO equalization," *Opt. Exp.*, vol. 23, no. 7, pp. 8409–842, Apr. 2015.

[16] W. Shieh, X. Yi, Y. Ma, and Q. Yang, "Coherent optical OFDM: Has its time come? [Invited]," *J. Opt. Netw.*, vol. 7, no. 3, pp. 234–255, Mar. 2008.

[17] W. Shieh, H. C. Bao, and Y. Tang, "Coherent optical OFDM: Theory and design," *Opt. Exp.*, vol. 16, no. 2, pp. 841–859, Jan. 2008.

[18] G. V. de Faria, M. R. Jimenez, and J. P. von der Weid, "PMD variations from factory to field in OPGW cabled fibers," *J. Lightw. Technol.*, vol. 18, no. 1, pp. 250–2522, Jan. 2006.

[19] J. D. Proakis and M. Salehi, *Digital Communications*.   New York, NY, USA: McGraw-Hill, 2008.